Geophys. J. Int. (1999) **139,** 657–670

Postglacial rebound and fault instability in Fennoscandia

Patrick Wu,[1] Paul Johnston[2] and Kurt Lambeck[2]

[1] *Department of Geology and Geophysics, University of Calgary, Alberta, Canada,* T2N 1N4. *E-mail: ppwu@acs.ucalgary.ca*
[2] *Research School of Earth Sciences, Australian National University, Canberra,* ACT 0200, *Australia*

Accepted 1999 June 18. Received 1999 April 27; in original form 1998 September 15

SUMMARY

The best available rebound model is used to investigate the role that postglacial rebound plays in triggering seismicity in Fennoscandia. The salient features of the model include tectonic stress due to spreading at the North Atlantic Ridge, overburden pressure, gravitationally self-consistent ocean loading, and the realistic deglaciation history and compressible earth model which best fits the sea-level and ice data in Fennoscandia. The model predicts the spatio-temporal evolution of the state of stress, the magnitude of fault instability, the timing of the onset of this instability, and the mode of failure of lateglacial and postglacial seismicity. The consistency of the predictions with the observations suggests that postglacial rebound is probably the cause of the large postglacial thrust faults observed in Fennoscandia. The model also predicts a uniform stress field and instability in central Fennoscandia for the present, with thrust faulting as the predicted mode of failure. However, the lack of spatial correlation of the present seismicity with the region of uplift, and the existence of strike-slip and normal modes of current seismicity are inconsistent with this model. Further unmodelled factors such as the presence of high-angle faults in the central region of uplift along the Baltic coast would be required in order to explain the pattern of seismicity today in terms of postglacial rebound stress. The sensitivity of the model predictions to the effects of compressibility, tectonic stress, viscosity and ice model is also investigated. For sites outside the ice margin, it is found that the mode of failure is sensitive to the presence of tectonic stress and that the onset timing is also dependent on compressibility. For sites within the ice margin, the effect of Earth rheology is shown to be small. However, ice load history is shown to have larger effects on the onset time of earthquakes and the magnitude of fault instability.

Key words: earthquakes, faulting, postglacial rebound, seismicity, stress.

1 INTRODUCTION

As a summary to the 1988 NATO Advanced Research Workshop on 'Causes and Effects of Earthquakes at Passive Margins and in Areas of Postglacial Rebound on both sides of the North Atlantic', Gregersen & Basham (1989) stated two outstanding issues in the study of intraplate earthquakes in Fennoscandia and Laurentia: the first one is the 'relative importance of plate tectonics and postglacial rebound in earthquake generation'; the second one is the postulated existence of a 'pulse of earthquake activity following deglaciation'.

Recent investigations of intraplate earthquakes in eastern Canada by Wu & Hasegawa (1996a,b) and Wu (1997) found that both tectonic forces and postglacial rebound stress are needed to explain current seismicity in the region. In their models, past tectonic processes have created zones of weakness in which current tectonic stresses bring pre-existing faults close to failure while glacial unloading reactivates optimally orientated faults. These models predict a pulse of earthquake activity at the end of deglaciation, with a timing and mode of failure that is consistent with observed patterns in most parts of eastern Canada (with the exception of Baffin Island) as well as with the contemporary stress orientations and the rotation in stress orientations since the end of deglaciation (see also Wu 1996, 1997, 1998b).

The situation in Fennoscandia appears to be different. First of all, seismicity is not limited to tectonic weak zones. In fact, most of the recent earthquakes with magnitude greater than 4 are distributed along the coastal regions (Fig. 1), while the interior is relatively non-seismic with most magnitudes less than 4 (Bungum 1989; Slunga 1989; Wahlstrom 1989; Bungum *et al.* 1991). Second, the throws of the postglacial faults in

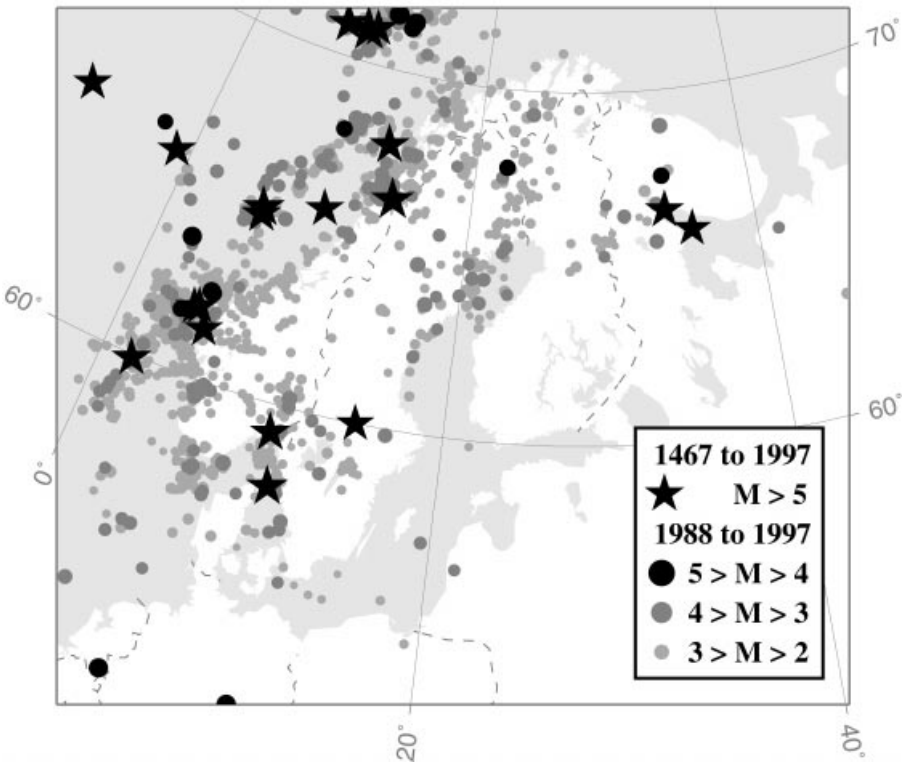

Figure 1. Seismicity map of Fennoscandia showing the magnitudes and locations of current and historic large earthquakes. Note that none of the earthquakes observed in Fennoscandia has a magnitude exceeding *M*6.1. (Data source: Institute of Seismology, University of Helsinki).

Fennoscandia are much larger than those in eastern Canada (Adams 1996; Shilts *et al.* 1992), and the mode of failure of current earthquakes in Fennoscandia is a mixture of strike-slip, normal and thrust motion (Slunga 1989; Wahlstrom 1989; Arvidsson 1996) whereas in eastern Canada it is mostly thrust motion (except in Baffin Island). Third, geologically determined uplift indicates that Canada is undergoing uplift caused solely by the ice unloading, while parts of Scandinavia may experience additional Neogene tectonic uplift (e.g. Rohrman *et al.* 1995).

Furthermore, theoretical study by Johnston *et al.* (1998) has shown that the magnitude of rebound stress depends on the wavelength of the load relative to the elastic thickness of the lithosphere, and thus the horizontal stresses in Fennoscandia are amplified when compared with those in Laurentia. A consequence of this is that any pulse of earthquake activity in Fennoscandia is predicted to occur about 2000 years before the end of deglaciation. The Johnston *et al.* (1998) model did not include the possible contribution to the stress field from any ambient background stress, and simplified the stress calculation by assuming that the mantle can be approximated by an incompressible medium. Moreover, only one viscosity model was considered in the study, and that viscosity–ice model pair does not give the optimum fit to observed sea level and ice data in Fennoscandia. More recently, a new rebound model, including a new ice sheet, has been proposed for Fennoscandia (Lambeck *et al.* 1998a). The purposes of this paper are: (1) to compute the temporal and spatial variation of stress and fault stability for the earth–ice model parameters proposed by Lambeck *et al.* (1998a), including an ambient tectonic stress field; (2) to investigate the sensitivity of these results (e.g. the state of crustal stress, the timing of past earthquakes and their mode of failure) to the effects of ambient stress, compressibility, mantle viscosity and ice model; and (3) to study the role that postglacial rebound stress might play in the generation of current earthquakes in Fennoscandia.

The present study differs from the earlier papers by Wu & Hasegawa (1996a,b) and Wu (1997, 1998a,b) in several respects: first, their area of interest was Laurentia (except in Wu 1998b) while the present study is for Fennoscandia. Second, the finite element approach was adopted while the spectral model of Johnston *et al.* (1998) is used here to give a higher resolution of rebound stress than is provided by the finite element method. Third, the range of earth and ice models explored by Wu (1997, 1998b) was restricted to a few special cases, and the combinations of earth and ice models used do not always give the optimal fit to all the observed sea level data in and around Laurentia.

The plan of the paper is as follows. Section 2 summarizes briefly some of the observational data for the seismicity and stress state of Fennoscandia. Section 3 discusses the stress model and reviews the measure used to define earthquake potential. Section 4 reviews the earth and ice models used. In Section 5.1, the results are presented for the optimum earth–ice model, and in the other subsections the effects of tectonic stress, mantle compressibility, viscosity and ice model are studied. Finally, these results are summarized in the Conclusion.

2 OBSERVATIONAL EVIDENCE

Fig. 1 illustrates the distribution of recent (1988–1997) seismicity of Fennoscandia, and the spatial pattern exhibits little correlation with the pattern of rebound for the region.

The mode of failure of the majority of the smaller earthquakes is a mixture of strike-slip, thrust and normal faulting (Slunga 1989; Wahlstrom 1989; Arvidsson 1996), also bearing little resemblance to what may be expected if the glacial unloading played a major role in the generation of this seismicity. (The strike-slip motion is consistent with tectonic stress being dominant, while thrust faulting is more consistent with a rebound origin.) Thus one could conclude that the past deglaciation has played at best only a minor role in generating current seismicity.

Present-day near-surface stress orientation measurements exhibit considerable variability (Stephansson 1989, 1993; Clauss *et al.* 1989), probably a consequence of local faults and topography. At depths below about 300 m the orientation of maximum horizontal stress becomes more consistent and occurs in a mainly NW–SE direction, in agreement with the direction of ridge push from the mid-Atlantic. Thus the dominant stress state appears to be of tectonic origin with contributions from rebound being of lesser importance.

The onset time of postglacial faults in Fennoscandia indicates that postglacial rebound may have played a much more important role in earthquake generation in Lateglacial and early Postglacial times. These postglacial faults (Fig. 2) are generally NNE–SSW-trending reverse faults (Kujansuu 1964; Lundqvist & Lagerbäck 1976; Lagerbäck 1978; Muir Wood 1989; Arvidsson 1996) which were formed 8000–9000 years ago (Lagerbäck & Witschard 1983; Arvidsson 1996). These faults are numerous, have displacements of up to 15 m and may have fractured the whole crust (Arvidsson 1996). Thus, Fennoscandia appears to have been more seismically active in the past, with events as large as magnitude 8 and stress drops of 5 MPa having occurred (Arvidsson 1996).

There is some evidence that suggests that rebound stress may still play a role in the generation of current seismicity: Ekman (1985, 1988) showed that there is a high spatial correlation between microseismicity and the maximum curvature of uplift, while a spatial correlation has also been suggested between the Gutenberg–Richter frequency–magnitude coefficient b and isolines of land elevation (Skordas & Kulhanek 1992).

In summary, onset timing and mode of failure of postglacial faults suggest that postglacial rebound may have played an important role in triggering faulting and earthquake activities during Lateglacial and early Postglacial times. However, it is not clear if rebound stress is still able to trigger seismicity in Fennoscandia today. By quantifying the crustal stress field, the rebound model results discussed below attempt to address some of these issues.

3 THE FAULT POTENTIAL MODEL

Changes in the stability of faults ($FSM^{(\delta)}$) are related to changes in the state of stress σ by

$$FSM^{(\delta)}(t) = FSM(t) - FSM(t_0)$$
$$= \frac{1}{2}\{[\sigma_1(t_0) - \sigma_3(t_0)] - [\sigma_1(t) - \sigma_3(t)]\}$$
$$+ \mu\beta\{[\sigma_1(t) + \sigma_3(t)] - [\sigma_1(t_0) + \sigma_3(t_0)]\} \quad (1)$$

(Wu & Hasegawa 1996a), where the spatial dependence has been suppressed,

$$\beta = \sin[\arctan(\mu)]/2\mu \quad (2)$$

and μ is the coefficient of friction taken to be 0.6; t is the time at which $FSM^{(\delta)}$ is calculated; t_0 is the initial time (before

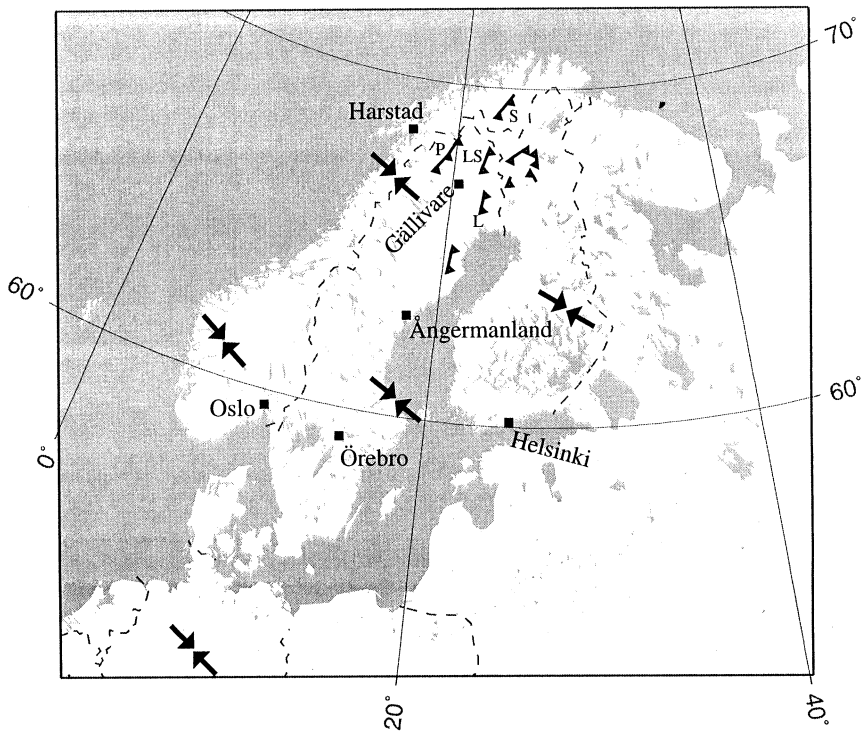

Figure 2. Map of Fennoscandia showing the distribution and orientation of some postglacial faults. L: Lansjärv fault; P: Pärvie fault; LS: Lainio–Suijavaara fault; S: Stuoragurra fault. Also plotted are the locations of the six sites in Figs 5 and 8 and the orientations of the first-order stress field indicated by the inward-pointing arrows.

the onset of glaciation at the last interglacial); and σ_1, σ_2, σ_3 are the maximum, intermediate and minimum (compressive) principal stresses, respectively. $FSM^{(\delta)}$ is a measure of fault potential: a negative value enhances the likelihood of faulting for optimally orientated virtual faults, whereas a positive value promotes fault stability. In some cases, when the faults are initially close to failure and optimally orientated (i.e. where the fault plane makes an angle of approximately 15°–25° to the horizontal), a small negative value of $FSM^{(\delta)}$ may be sufficient to trigger an earthquake. However, most postglacial thrust faults in Fennoscandia are high-angle faults and are not optimally orientated. To reactivate them requires a large negative value of $FSM^{(\delta)}$ (see Fig. 2c in Wu 1998a). In other cases, the initial value of FSM is positive and not zero (i.e. all faults in a region are more than marginally stable). Then even optimally orientated faults require large and negative values of $FSM^{(\delta)}$ to overcome the initial stability and to trigger earthquakes. For optimally orientated faults, the mode of failure depends on which of the principal stresses is closest to the vertical. If σ_1 is nearly vertical, then the mode of failure is normal; if σ_3 is close to the vertical, then thrusting occurs; otherwise, the mode of failure is strike-slip.

The total stress is assumed to be composed of the rebound stress, tectonic stress and overburden stress. The orientation of the first-order tectonic maximum horizontal principal stress is taken to be in the N60°W direction (Stephansson 1989, 1993; Clauss *et al.* 1989), but the magnitudes of these tectonic stresses are largely unknown. However, tectonic stress magnitudes have little effect on $FSM^{(\delta)}$ (Wu & Hasegawa 1996a,b), and only their stress difference affects the total stress orientation. In this paper, the maximum horizontal tectonic stress is taken to be 150 MPa, such that the total stress at 12.5 km depth approaches the level of stress deduced by Zoback *et al.* (1994) for the mid-crustal region, while a range of minimum horizontal tectonic stresses will be considered.

4 MANTLE AND ICE MODELS

Rebound stress is calculated with the spectral method described in Johnston *et al.* (1998). The Earth is modelled as a spherical, Maxwell viscoelastic body with depth-dependent density and elastic parameters given by the seismological model PREM (Dziewonski & Anderson 1981). It includes an elastic lithosphere of thickness H_1, a mantle with different effective viscosities above and below the 670 km seismic discontinuity, and an inviscid core. All of the earth models are compressible except for the one example illustrated in Fig. 4(b) below.

The surface load consists of one cycle of glaciation and deglaciation and the concomitant changes in ocean loading, the latter obtained by solving the self-consistent sea-level equation (e.g. Mitrovica & Peltier 1991). For the earth models considered here, earlier glacial cycles are of little importance if the stress field predictions are limited to the last phase of deglaciation. The glaciation phase is approximated by a linear growth period from 110 ka BP to 20 ka BP, with the ice margin advancing with time. This is followed by a more realistic deglacial phase which begins at 18 ka BP. Two different models for this latter stage will be used.

The first is a 'cold-based' ice sheet in which the radial transects of the ice thickness are quasi-parabolic and the ratio of the maximum ice thickness to the square root of transect length is proportional to the basal shear stress (Paterson 1981). The ice thickness at the time of the Last Glacial Maximum (LGM) is taken from Denton & Hughes (1981), and the ice retreat margins are taken from Andersen (1981) and Pedersen (1995). The ice model over the British Isles is that of Lambeck (1995). From the maximum ice height and the ice margin location at the LGM, effective basal stress conditions can be estimated for radial transects, and ice thicknesses during the subsequent retreat stage are computed on the assumption that basal shear conditions along any radial profile remain unchanged through time (Lambeck 1993). Thus the parabolic profiles are retained throughout the retreat stage. However, Lambeck *et al.* (1990) found that the ice thicknesses proposed by Denton & Hughes (1981) significantly overestimated the rebound in Lateglacial times and scaled the ice model by a single parameter (γ) that was estimated, along with the earth model parameters, from the inversion of the sea-level data. The analyses led to an optimum combination of earth–ice model parameters for which $\gamma \approx 0.6$, such that the maximum ice heights over Scandinavia are estimated to have been only about 2000 m. This scaled ice model is referred to here as SCAN-1 and will be used to explore the sensitivity to ice load in Section 5.5.

More detailed analyses of the observational evidence identified some major inadequacies of the SCAN-1 ice model, particularly in the eastern and southern parts of the ice sheet where, for a wide range of plausible earth models, the scaled 'cold-based' ice sheets lead to an opening of the Baltic Sea to the Arctic Ocean in Lateglacial and Postglacial times, inconsistent with field evidence. Likewise, this model leads to a sequence of isolation and flooding events of the Baltic that is incompatible with the observed history of the basin unless the ice thickness is further reduced over the southern regions (Lambeck 1999). Also, the discrepancies between predicted and observed sea-level change based on the SCAN-1 class of models are very large, irrespective of earth model, unless the ice thickness over southeastern and southern Fennoscandia is reduced substantially. Thus in the next iteration of the rebound solution, the γ parameter was assumed to be regionally variable, and the inversion of the sea-level data was carried out for earth model parameters as well as for a series of γ parameters that provided the basis for a regional scaling of the initial ice sheet. This produced the ice model SCAN-2 (Lambeck *et al.* 1998a), which can be characterized as cold-based in the north and west, and warm-based or loosely coupled to the subglacial surface in the south and east, consistent with geomorphological indicators (Kleman *et al.* 1997). This model leads to a much improved agreement between observed and predicted shoreline elevations throughout the Scandinavian region, and, while it could be argued that the resulting ice model is dependent on the choice of rheological parameters for the mantle, all plausible earth models lead to similar conclusions about the ice sheet properties, as do tests based on independent data sets (Lambeck *et al.* 1998b; Lambeck 1999). The SCAN-2 deglaciation history is contoured in Fig. 3 for three discrete time steps although the actual model is defined at 1000 yr intervals.

The resulting optimum earth model, E1, is defined in Table 1, and the SCAN-2/E1 combination is taken to be the reference model in Section 5.1 to study the role rebound stress plays in triggering earthquakes and in Sections 5.2 and 5.3 to explore the effects of incompressibility and tectonic stress. In Section 5.4, SCAN-2 is used with a series of other earth-model

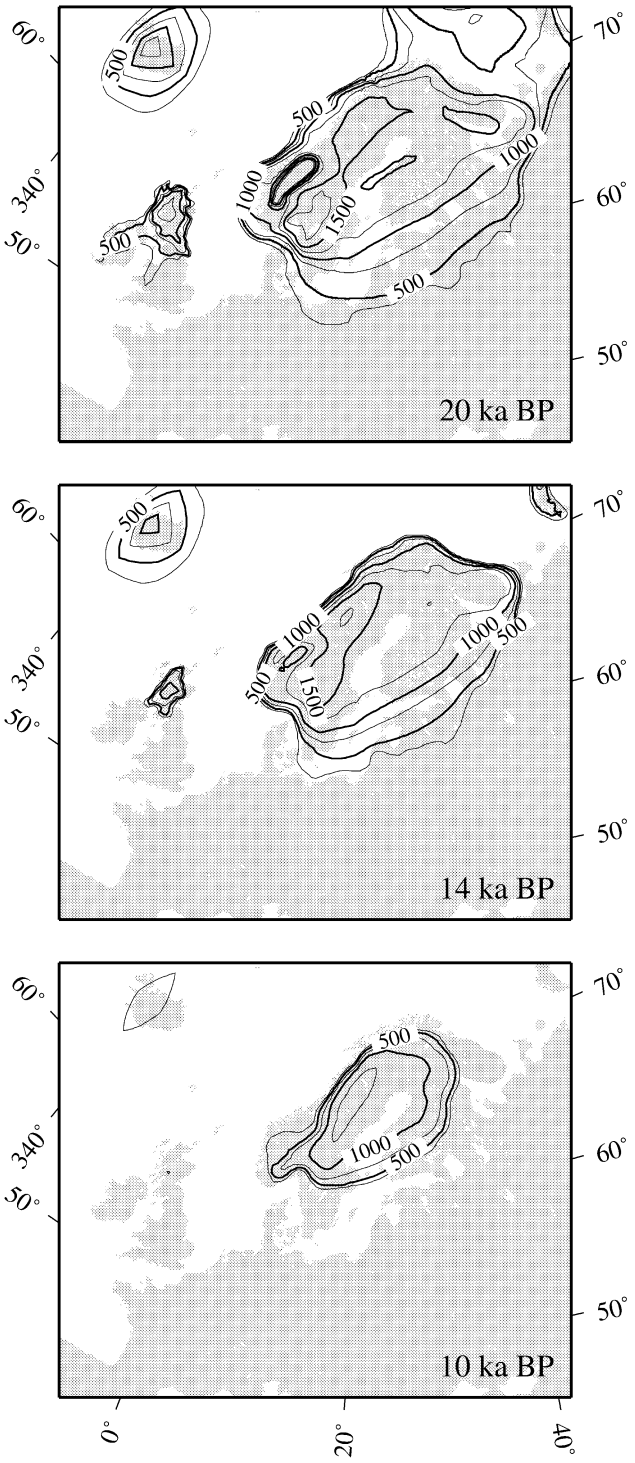

Figure 3. SCAN-2 deglaciation history used to calculate the spatio-temporal pattern of rebound and associated stress for Earth model E-1 (Table 1). Contours are ice thicknesses in metres.

parameters (E2–E7) given in Table 1 to explore systematically the range of mantle viscosities acceptable by geological data. Models E2 and E3 explore the dependence of the stress field on lithospheric thickness, models E4 and E5 explore this dependence on upper mantle viscosity, and models E6 and E7 examine this dependence on lower mantle viscosity.

Table 1. Earth–ice models used in Figs 7, 9 and 10.

Model Name	lithospheric thickness (km)	upper mantle viscosity ($\times 10^{21}$ Pa s)	lower mantle viscosity ($\times 10^{21}$ Pa s)	Ice Model (SACAN no.)
E-1	75	0.36	8	2
E-2	65	0.36	8	2
E-3	85	0.36	8	2
E-4	75	0.29	8	2
E-5	75	0.45	8	2
E-6	75	0.36	6	2
E-7	75	0.36	13	2
E-1	75	0.36	8	1

5 RESULTS

In the following, all stress orientation and stress rotation calculations correspond to the Earth's surface, where the measurements are made. In contrast, results for the fault stability and related calculations are for a representative depth of 12.5 km, corresponding to the typical depth of crustal earthquakes (Slunga 1989). However, the conclusions of this paper are valid for depths within the top 40 km (Wu & Hasegawa 1996a; Johnston *et al.* 1998).

5.1 Predictions of stress for the reference earth–ice model parameters

In this subsection, the reference model E1 (compressible earth with tectonic stress) with SCAN-2 is used to study the state of stress, fault stability and the role postglacial rebound stress might play in the generation of current earthquakes in Fennoscandia.

Fig. 4(a) shows the spatio-temporal variation of $FSM^{(\delta)}$ at glacial maximum (20 ka BP), at the end of deglaciation (9 ka BP) and at the present (0 ka BP) for this reference model. Fig. 5 shows the temporal variation of the principal stresses (expressed in terms of horizontal principal stresses S_{Hmax}, S_{Hmin} and the vertical principal stress *PrinZ*), $FSM^{(\delta)}$ and the mode of failure for the six sites in Fennoscandia identified in Fig. 2.

Inspection of Figs 4(a) and 5 shows that, at 20 ka BP, fault stability is predicted underneath the ice load in Fennoscandia because the increase in mean stress requires a larger stress difference to cause failure, as is shown by the movement of the Mohr circle away from the failure line (Johnston 1987, 1989). Beyond the ice margin, instability is predicted because rebound stress there is tensional. In contrast to the case for Scandinavia, fault instability is predicted beneath the smaller load over the British Isles due to the interaction between this local stress field and the stress field caused by the nearby Fennoscandian ice sheet (Johnston *et al.* 1998, 1999).

By 9 ka BP, instability occurs all over Fennoscandia and the British Isles (Fig. 4). This early onset of instability before complete deglaciation of Scandinavia is due to the amplification of stress as the wavelength of the load decreases towards the flexural wavelength of the lithosphere (Johnston *et al.* 1998). In Fig. 5, the vertical stress is the minimum principal stress in all examples, and any failure is predicted to occur by thrust faulting. This is consistent with the fact that most observed postglacial faults are reverse faults. According to Arvidsson (1996), these observed faults were probably formed

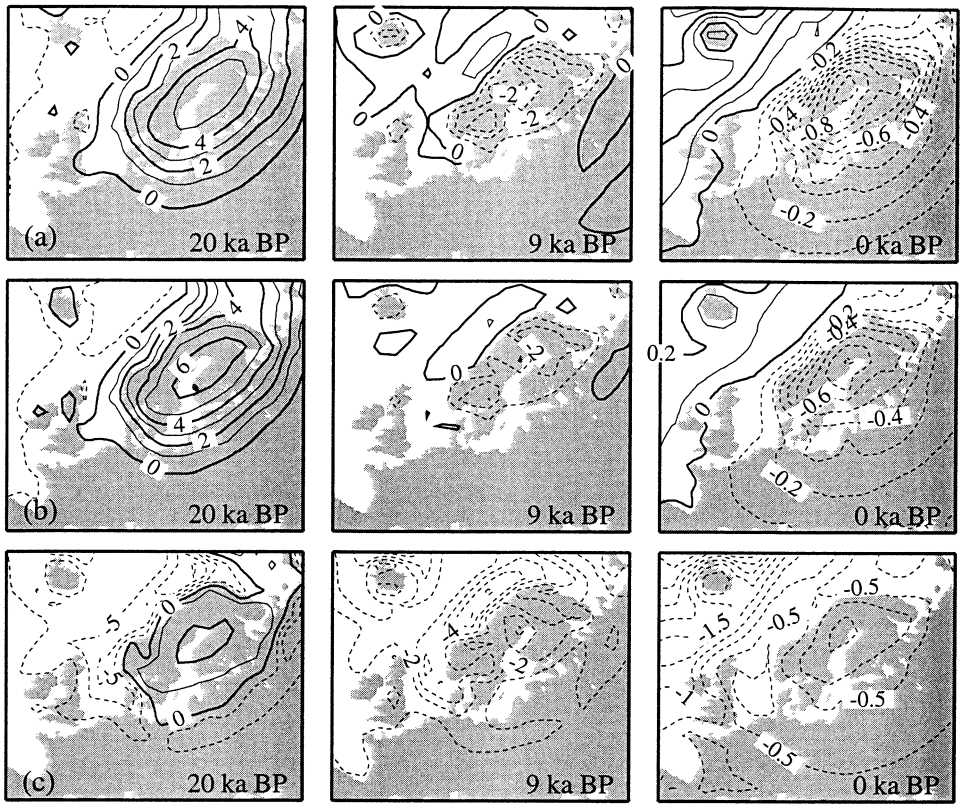

Figure 4. The spatio-temporal variation of $FSM^{(\delta)}$ in Fennoscandia is shown at three time periods for the earth model E-1 and ice model SCAN-2. Contour labels are in MPa. Contours in the dashed lines have negative values. In the top row (a), the full model includes compressibility and tectonic stress. The difference between row (a) and the middle row (b) is that an incompressible earth model is considered in (b). Similarly, the lower row (c) differs from (a) in that tectonic stress is neglected in (c).

by single events, with magnitude as high as $M_w = 8.2$, extending through most of the crust. Fig. 5 also shows that fault instability over Scandinavia starts at around 13–9 ka BP and maximum instability is reached at around 11–9 ka BP for all sites. For the Pärvie fault near Gällivare, the estimated age of faulting is 9 ± 1 ka BP, consistent with that predicted by the present model.

The magnitude of maximum instability is largest near Gällivare, the area around which most postglacial faults are found. There, the magnitude is predicted to be about 5 MPa at around 8 ka BP, about five times larger than that predicted for Laurentia. If these values of fault instability are indicators of the magnitude of rebound stress available to trigger earthquakes, then this larger magnitude of $FSM^{(\delta)}$ may result in larger throws of the postglacial faults in Fennoscandia, assuming that rock friction for fault reactivation in Laurentia is comparable with that in Fennoscandia (Johnston *et al.* 1998).

At the present time (0 ka BP), fault instability is predicted over all of Fennoscandia and the northern part of the British Isles. A maximum instability of about 1 MPa is predicted near the centre of rebound at the present (Fig. 4a), and the predicted mode of failure is thrusting (Fig. 5). However, these predictions are not consistent with the observed evidence for recent faulting. First, the mode of failure of current earthquakes (which have magnitudes of no more than 6.1) is not restricted to thrusting (Arvidsson 1996; Arvidsson & Kulhanek 1994), indicating that tectonic stress may play a comparatively more significant role today than at the end of deglaciation because rebound stress relaxes with time after deglaciation. Second, unlike the prediction of present fault instability (Fig. 4a), Fig. 1 shows that the centre of rebound is relatively non-seismic. The larger earthquakes are mostly located around the coastal regions and along the fault zones in the North Sea and North Atlantic, where the seismicity is mostly due to tectonics.

Three somewhat *ad hoc* scenarios are considered as the kinds of conditions that are required to explain both the distribution of earthquakes along the coast and the lack of large-magnitude seismicity within the centre of rebound today, and which explain at the same time the occurrence of large earthquakes near the end of deglaciation. The first scenario assumes that the value of the *FSM* before the onset of glaciation (i.e. the initial value) is close to zero along the coast but is about 2 MPa within the centre of rebound. In the second scenario, an $FSM^{(\delta)}$ of about -2 MPa is assumed to be required to activate the high-angle faults near the centre of rebound but the pre-existing faults near the coast are assumed to be optimally orientated and close to failure. Under both scenarios, fault instability cannot be initiated until the value of $FSM^{(\delta)}$ falls below -2 MPa. Thus, the rebound stress available today is not large enough to trigger earthquakes near the centre of rebound because either the initial fault stability or the fault angle is too high. The third scenario is similar to the first two except that the stress released along faults early in the deglaciation stage is used to explain the lack of seismicity within the centre of rebound today. It assumes that the optimally orientated or high-angle faults require about -2 MPa

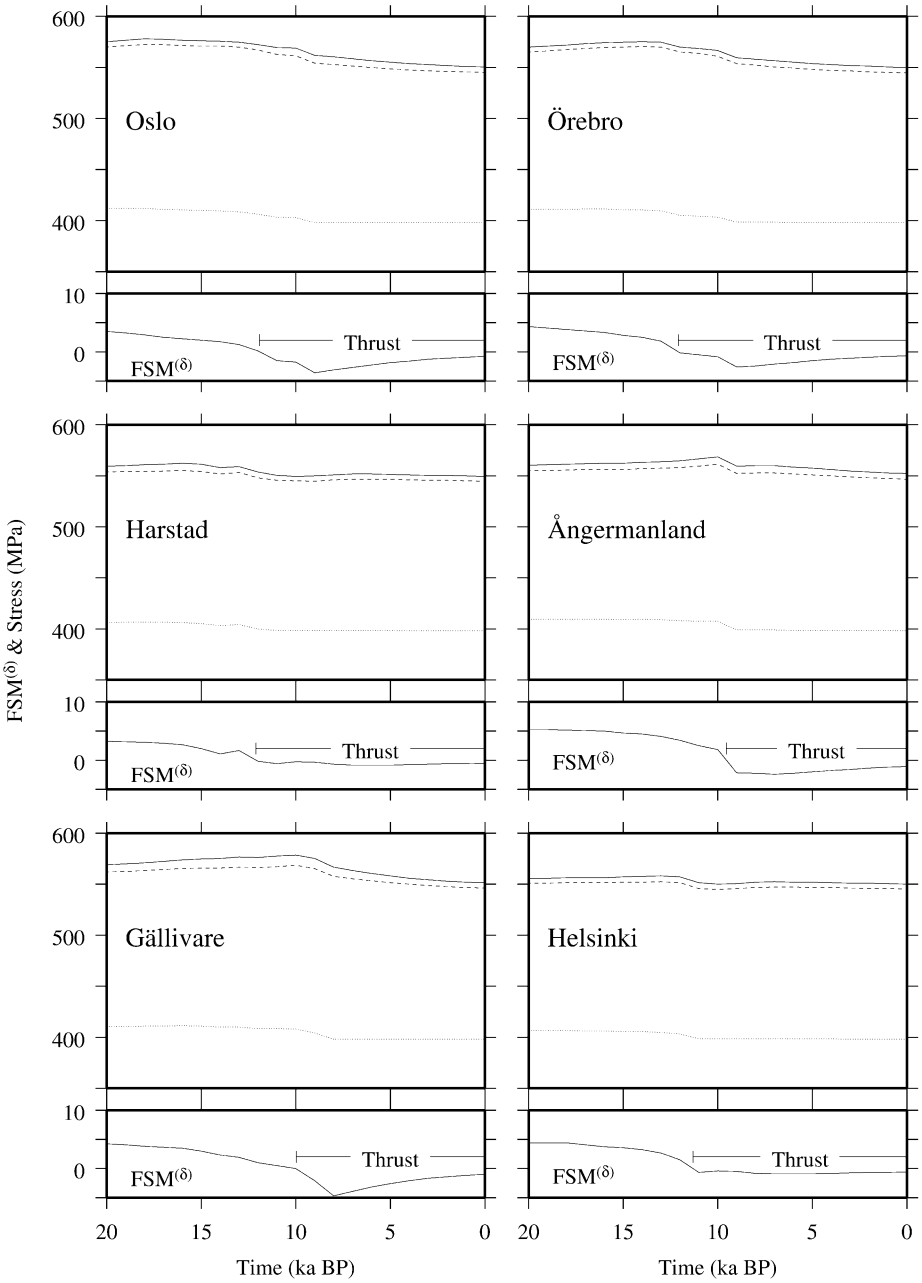

Figure 5. Evolution of the horizontal principal stress S_{Hmax} (solid line), S_{Hmin} (dashed line), the vertical principal stress *PrinZ* (dotted line), $FSM^{(\delta)}$ and the mode of failure for the six sites in Fig. 2, all at a seismogenic depth of 12.5 km for compressible earth model E-1 and ice model SCAN-2.

of $FSM^{(\delta)}$ to be reactivated. For a large earthquake, the stress released would have caused the negative value of $FSM^{(\delta)}$ to jump to zero or to some small positive value. If $FSM^{(\delta)}$ continued to increase after faulting, then the faults are predicted to remain stable and no earthquakes are generated today. This is assumed to have occurred at sites such as Ångermanland and Gällivare, where $FSM^{(\delta)}$ increases by several megapascals between Lateglacial times and the present. However, for coastal sites where the large postglacial earthquakes did not occur, $FSM^{(\delta)}$ remains negative and so larger earthquakes could occur today under this set of initial conditions. It should be noted that for all three scenarios (or combinations of them), the increased value of $FSM^{(\delta)}$ needed to trigger earthquakes results in a better fit between the predicted (see Gällivare in Fig. 5) and the observed onset time of seismicity.

The orientation and magnitude of the horizontal principal stress is illustrated in Fig. 6 for a tectonic stress difference (S_{Hmax}–S_{Hmin}) of 5 MPa. At 9 ka BP, the orientation of the maximum principal stress (solid lines in Fig. 6a) is non-uniform in Fennoscandia, ranging from E–W north of Harstad to N–W near the centre of rebound and again to more E–W in southern Sweden. The predicted palaeostress orientation near Gällivare is consistent with palaeostress orientations inferred from the nearby postglacial faults. However, any contribution to S_{Hmax} from ridge push at the North Atlantic is aligned approximately in the N–W direction also, and may form the dominant

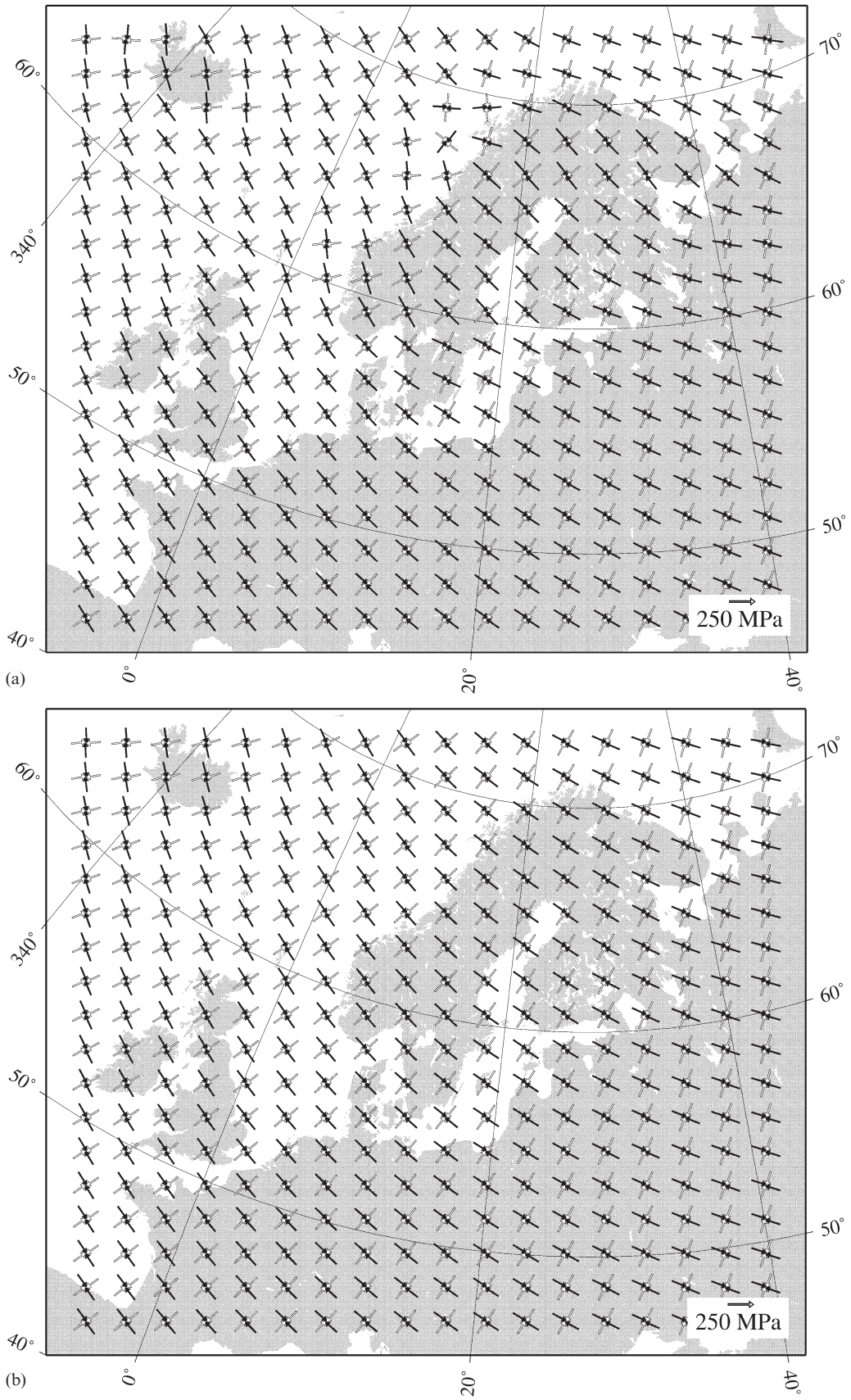

Figure 6. Orientation and magnitude of the projected horizontal principal rebound stresses (a) 9000 years ago and (b) at present for the reference ice–earth model (compressible E-1 and SCAN-2) that includes tectonic stress. Solid lines indicate the direction of maximum horizontal stress and hollow lines indicate the minimum horizontal stress.

contribution to the observed stress orientations. Stress orientations predicted for the present epoch are more uniform, reflecting the dominance of the NW-orientated background tectonic stress field over the rebound contribution to stress and are consistent with the orientation of the first-order stress field observed in Fennoscandia today (Stephansson 1989, 1993; Clauss *et al.* 1989).

The top two frames of Fig. 7 illustrate the orientation of S_{Hmax} for the reference model at two epochs, with varying magnitude of the minimum horizontal tectonic stress. For regional tectonic stress differences less than about 8 MPa, the left side of Fig. 7 shows that the rebound stresses in the Lateglacial period dominate. For tectonic stress differences of 1–8 MPa, significant stress rotation can occur during the last 9 ka as the rebound stresses relax (as can be seen by comparing Figs 6a and b). At 9 ka the stress orientation is generally non-uniform with a maximum difference in orientation between Harstad and Oslo of about 90°, but for the present epoch the stress orientation is uniform. For tectonic stress differences greater than about 8 MPa, tectonic stress completely determines the stress orientations, and thus a uniform stress field is predicted for Lateglacial times and little rotation in stress orientation is predicted for the last 9 kyr.

For small tectonic stress differences (<1 MPa), rebound stresses dominate the present stress orientation and the stress field remains non-uniform in Fennoscandia throughout the postglacial period. However, this latter scenario is not consistent with the observed present stress orientations, which show a

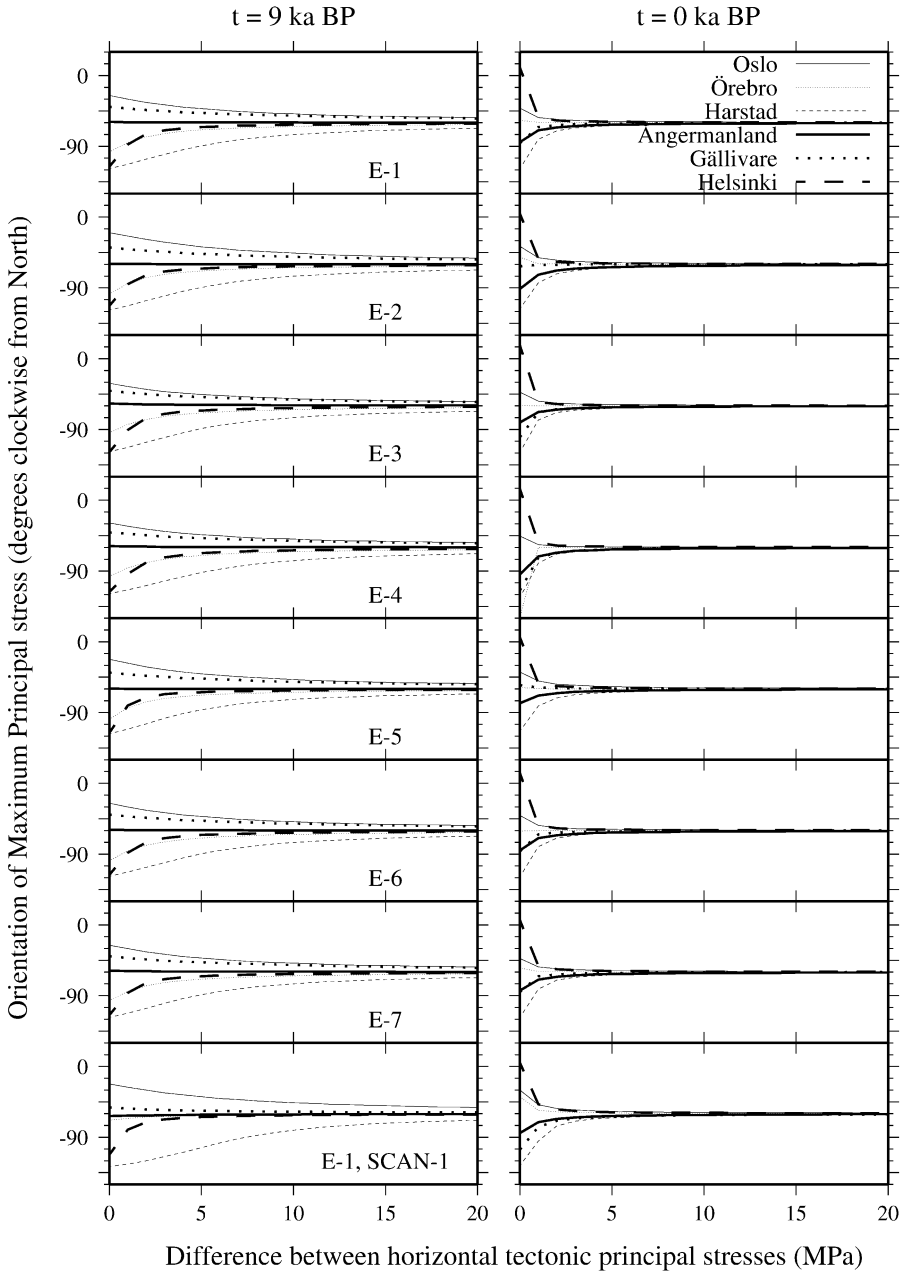

Figure 7. The effect of tectonic stress difference on the orientation of S_{Hmax} for the six sites is shown for models E1–E7 (Table 1) with the SCAN-2 ice model, and E-1 with SCAN-1 ice model.

fairly uniform NW orientation below 300 m depth, indicating that the regional stress field now dominates. Palaeostress observations for Fennoscandia are, however, insufficient to establish whether significant stress rotation has occurred during the last 9 ka.

In summary, the ice–earth model is able to explain the observed timing and mode of failure of the postglacial faults in Fennoscandia. The rate of decay of rebound stress predicted by this model is fast enough so that tectonic stress is predicted to dominate the current stress orientation, as is observed. At present, fault instability up to 1 MPa is predicted in Fennoscandia, and this magnitude of instability may trigger current seismicity, yet the rebound model predicts a predominance of thrust faulting which is not observed. Finally, three scenarios have been proposed to explain the lack of current seismicity near the centre of rebound. Until more information about local fault properties (e.g. dip angle, initial *FSM*, etc.) and rebound stress build-up at these fault is known, however, these scenarios remain purely speculative.

5.2 Effects of mantle compressibility

Johnston *et al.* (1998) considered only incompressible earth models in their study of fault instability in Fennoscandia. Fig. 4(b) shows the spatio-temporal variation of $FSM^{(\delta)}$ when an incompressible E1 model is used instead of a compressible model (Fig. 4a). A comparison of Figs 4(a) and (b) shows that, at 20 ka BP, the location of the zero contour does not change significantly, except that western Scotland and part of Ireland become more stable. In addition, the magnitude of $FSM^{(\delta)}$ near the centre of rebound increases from 5 to 6 MPa. At 9 ka BP, the offshore region between Fennoscandia and Iceland becomes less stable. In contrast, the centre of rebound becomes slightly less unstable. This is also true at 0 ka BP.

Thus, overall, the main effect of incompressibility is to decrease the amplitude of $FSM^{(\delta)}$ in and around Fennoscandia. Although this may impact upon the timing of rebound-generated earthquakes in the British Isles and offshore, it has little effect on the onset time of instability nor on the mode of failure within Fennoscandia.

5.3 Effects of neglecting tectonic stress

The spatio-temporal variation of $FSM^{(\delta)}$ for the model illustrated in Fig. 4(a) without the tectonic stress component is shown in Fig. 4(c), and the temporal variation of the principal stresses, $FSM^{(\delta)}$ and the mode of failure are shown in Fig. 8.

A comparison of Figs 4(a) and (c) shows that tectonic stress has a very large effect on the spatio-temporal variation of $FSM^{(\delta)}$—not only is the magnitude of $FSM^{(\delta)}$ affected, but the location of the zero contour is also changed drastically. For example, with tectonic stress neglected, the model in Johnston *et al.* (1998) predicts strike-slip faulting in Scotland and normal faulting in England today, but, with the inclusion of tectonic stress, the model predicts thrust faulting at these localities (Johnston *et al.* 1999). For sites within the ice margin, however, thrusting is predicted by models with and without tectonic stress. Furthermore, from a comparison of Figs 5 and 8, the neglect of tectonic stress is seen to have only minor effects on the onset time of instability and its magnitude there.

Thus, although tectonic stress strongly affects the value of $FSM^{(\delta)}$ and the mode of failure outside the ice margin, its effects are relatively minor within central Fennoscandia, and the conclusions of Johnston *et al.* (1998) are confirmed. (We will continue to include tectonic stress in all other models of this paper.)

5.4 Effects of viscosity variations

In Section 5.1, it was shown that the onset time of faulting, the mode of failure and the contemporary stress orientation can all be attributed to the stress field that was generated by glacial unloading. However, the predicted stress field is likely to be earth-model-dependent (Spada *et al.* 1991), and the aim here is to examine systematically the dependence of the stress-field characteristics on the values chosen for lithospheric thickness and upper and lower mantle viscosities by using the compressible earth models E1–E7 (Table 1) based on the ice model SCAN-2. The earth models cover the range of parameters that yield sea-level predictions that are consistent with the observational evidence (Lambeck *et al.* 1998a).

It can be shown that viscosity variations have no effect on the mode of failure (Wu 1997). Thus, for the models below, we shall focus on the effects of mantle viscosity on (1) the onset time of earthquakes; (2) the minimum value of $FSM^{(\delta)}$ and (3) stress rotation. The results are summarized in Figs 9, 10 and 7, respectively.

Inspection of Fig. 9 shows that the main variation in the predicted onset time for the various sites is a function of their location with respect to the former ice margin. For example, for sites close to the ice margin, the onset time is earlier (e.g. $\sim$12 ka BP in Oslo, Örebro and Harstad) than for sites nearer to the centre of rebound (e.g. $\sim$9.8 ka BP in Gällivare). This is a consequence of the retreat in ice margin as the Fennoscandian ice melted. Fig. 9(c) shows that an increase in lithospheric thickness generally leads to an earlier predicted onset time, although this dependence is weak. Increasing the upper mantle viscosity (Fig. 9a) results in a delay in the predicted onset time, but again the delay is small for the range of values considered. Finally, it can be seen that onset time is generally insensitive to lower mantle viscosity in Fennoscandia, due to the fact that the lower mantle is not strongly deformed by the Fennoscandian ice sheet (e.g. Mitrovica 1996).

Fig. 10 shows that the predicted minimum $FSM^{(\delta)}$ at a site is generally influenced by (1) its distance from the ice margin and (2) Earth rheology. In general, sites that lie close to the former ice margin (e.g. Harstad and Helsinki) have the smallest magnitude of minimum $FSM^{(\delta)}$ (<1 MPa), for sites near the centre of rebound (e.g. Ångermanland) the magnitude is slightly larger (about 2 MPa), and sites lying between the centre and the ice margin have the largest magnitude (about 4.5 MPa in Gällivare). Generally, an increase in lithospheric thickness results in a smaller minimum in $FSM^{(\delta)}$, except for the sites in Ångermanland and Oslo. An increase in upper mantle viscosity also results in a smaller minimum in $FSM^{(\delta)}$ except at Örebro. Again, due to the relatively small size of the Fennoscandian ice sheet, lower mantle viscosity has little effect on the value of $FSM^{(\delta)}$.

Finally, the effect of tectonic stress difference (S_{Hmax}–S_{Hmin}) on changes in orientation of the horizontal principal stress is plotted in Fig. 7. Overall, it shows that the range of lithospheric thickness and upper and lower mantle viscosity variations allowed by the geological data have only minor effects on

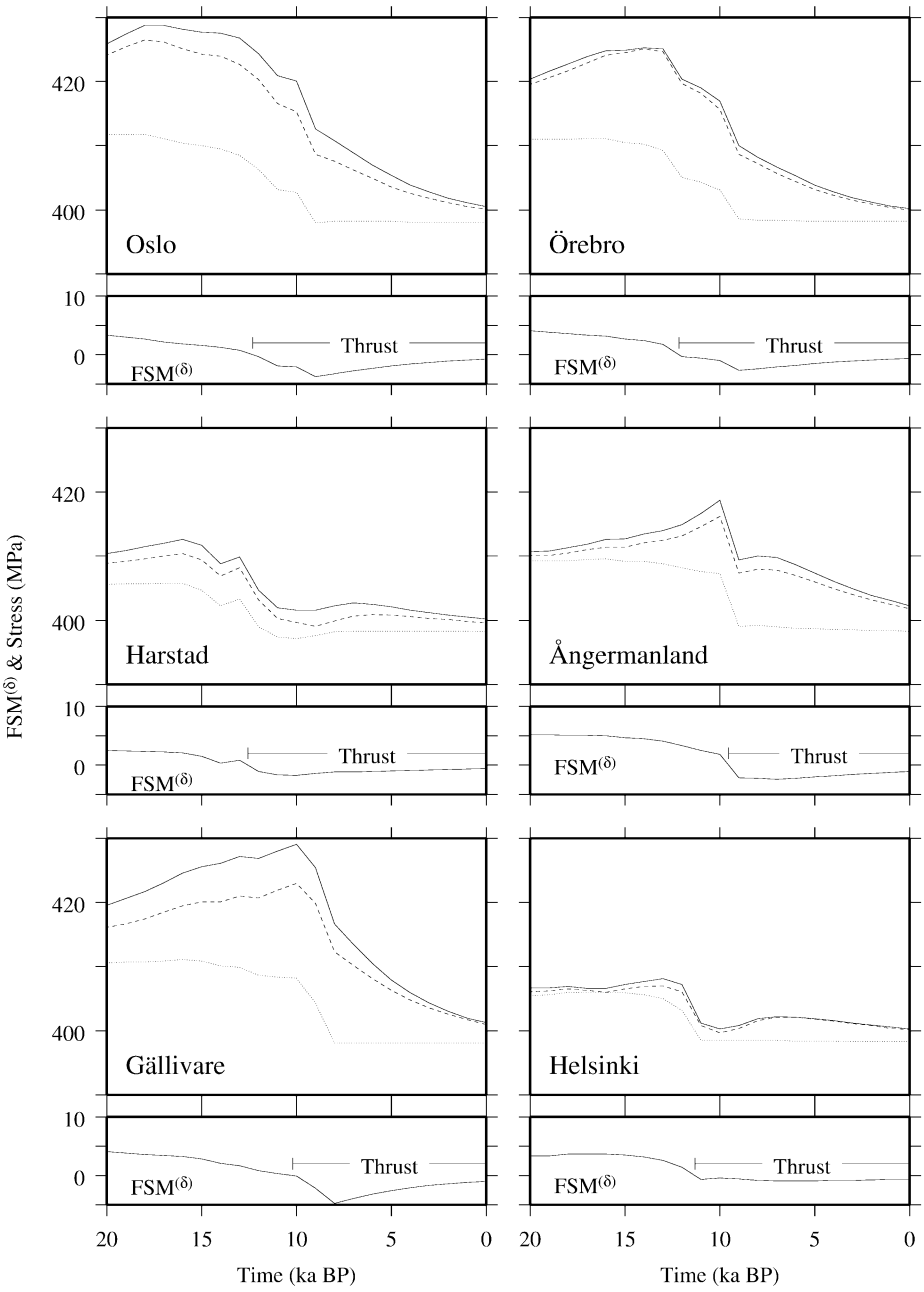

Figure 8. As Fig. 5, except that no tectonic stress is used in this calculation.

stress orientation. As discussed in Section 5.1, stress rotation during the last 9 ka can occur if the tectonic stress difference is between 1 and 8 MPa. However, stress rotation has not been established in Fennoscandia, and thus, until more palaeo-stress orientation data become available, these results remain only of theoretical interest.

5.5 Effects of ice model

So far, SCAN-2 has been the only ice model considered because, in combination with the viscosity model E1, it predicts the observed rebound signatures well. In order to study the effects of the ice model, the compressible earth model E1 is used with the cold-based SCAN-1 ice model. The results are summarized in Figs 9(d,) 10(d) and 7. Inspection of these figures shows that changing the load history may significantly alter the stress orientation, the onset time of sites near the ice margin (e.g. Harstad) and the minimum value of $FSM^{(\delta)}$ for sites near the centre of rebound (e.g. Ångermanland). The main difference between the ice models SCAN-1 and SCAN-2 is that SCAN-1 is thinner in the west of Fennoscandia than SCAN-2 but thicker in the east. This is reflected in the predictions of minimum $FSM^{(\delta)}$ in Fig. 10(d), where the western sites Oslo, Örebro and Harstad have smaller values of the minimum $FSM^{(\delta)}$ for SCAN-1 than for SCAN-2, but the eastern sites have larger values.

The difference between the two sets of predictions shows that a proper choice of ice load (i.e. one that best fits geological data as in SCAN-2) is important in the study of earthquake onset time, minimum $FSM^{(\delta)}$ and stress orientation.

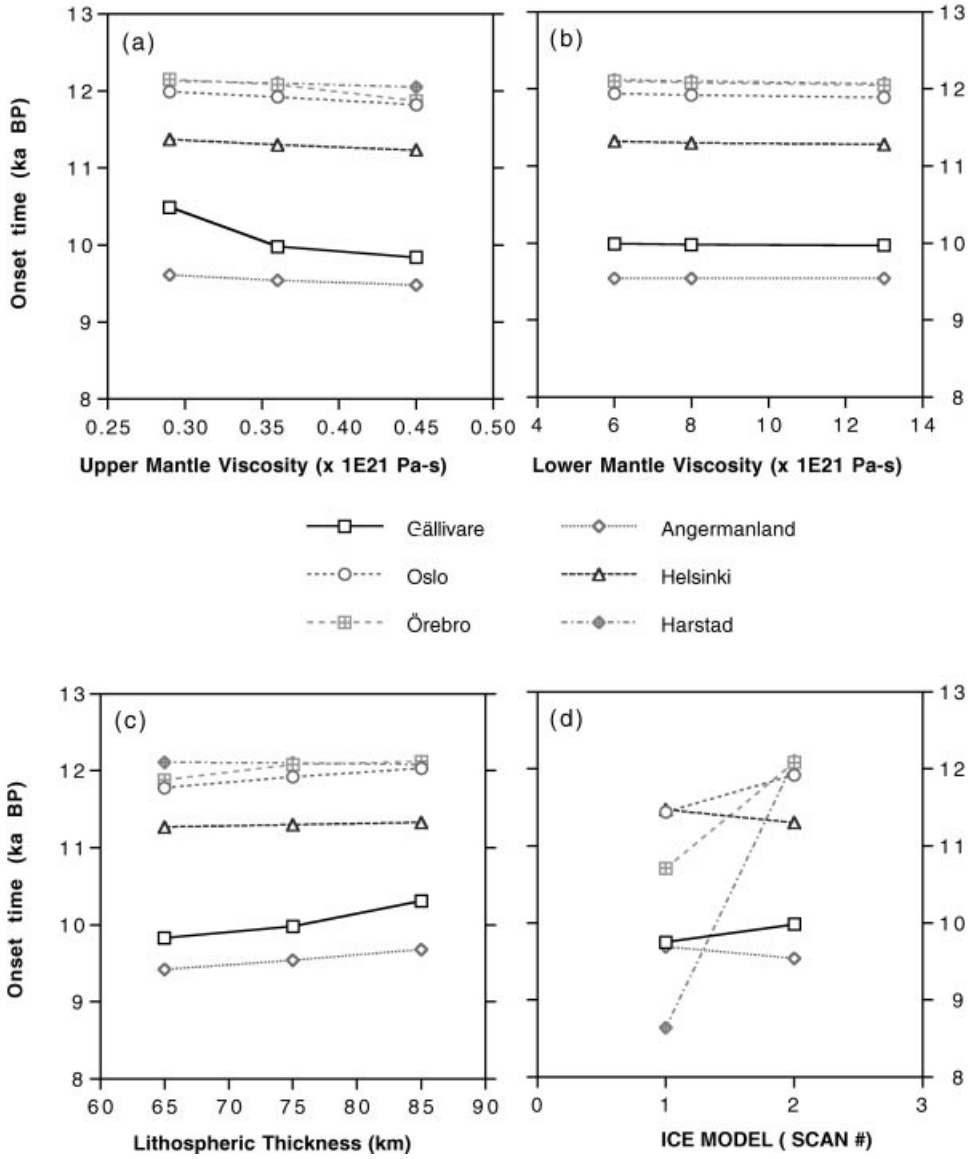

Figure 9. Effect of lithospheric thickness, upper and lower mantle viscosity and ice model on earthquake onset time for the earth–ice models in Table 1.

6 CONCLUSIONS

This paper has examined whether the Late Pleistocene deglaciation of Scandinavia can have led to seismic activity in the region as a result of the changing crustal stress regime. In particular, the effects of mantle rheology, compressibility, tectonic stress and ice load on a number of variables (onset timing, the mode of failure, stress orientation and the amount of stress available in triggering seismicity) have been investigated for a range of model parameters. It is found that the effects of mantle rheology and compressibility on these predicted variables are generally small within the range of parameters permitted by geological data. Tectonic stress, assumed to be compressive with a maximum horizontal stress of 150 MPa in the N60°W direction, strongly affects the mode of failure predicted outside the ice margin; however, its effect on the predictions within the ice margin is small since it is the rebound stress there that dominates the total stress field. The largest effect is due to the ice model and indicates that a proper choice of ice load is crucial in the study of earthquake onset timing.

With optimum ice and earth model parameters inferred from sea-level and ice data, predictions of the observed timing, the mode of failure of the postglacial faults and the current stress orientations in Fennoscandia are all consistent with the observations. The models also predict that present-day $FSM^{(\delta)}$ is of the order of 1 MPa in Fennoscandia, which is sufficient to trigger seismicity today; however, more information on local fault and stress properties is required in order to understand the modern seismicity pattern and mode of failure in terms of rebound stress.

ACKNOWLEDGMENTS

This work was supported by a grant to PW from NSERC of Canada. We are also indebted to Dr J. X. Mitrovica and an

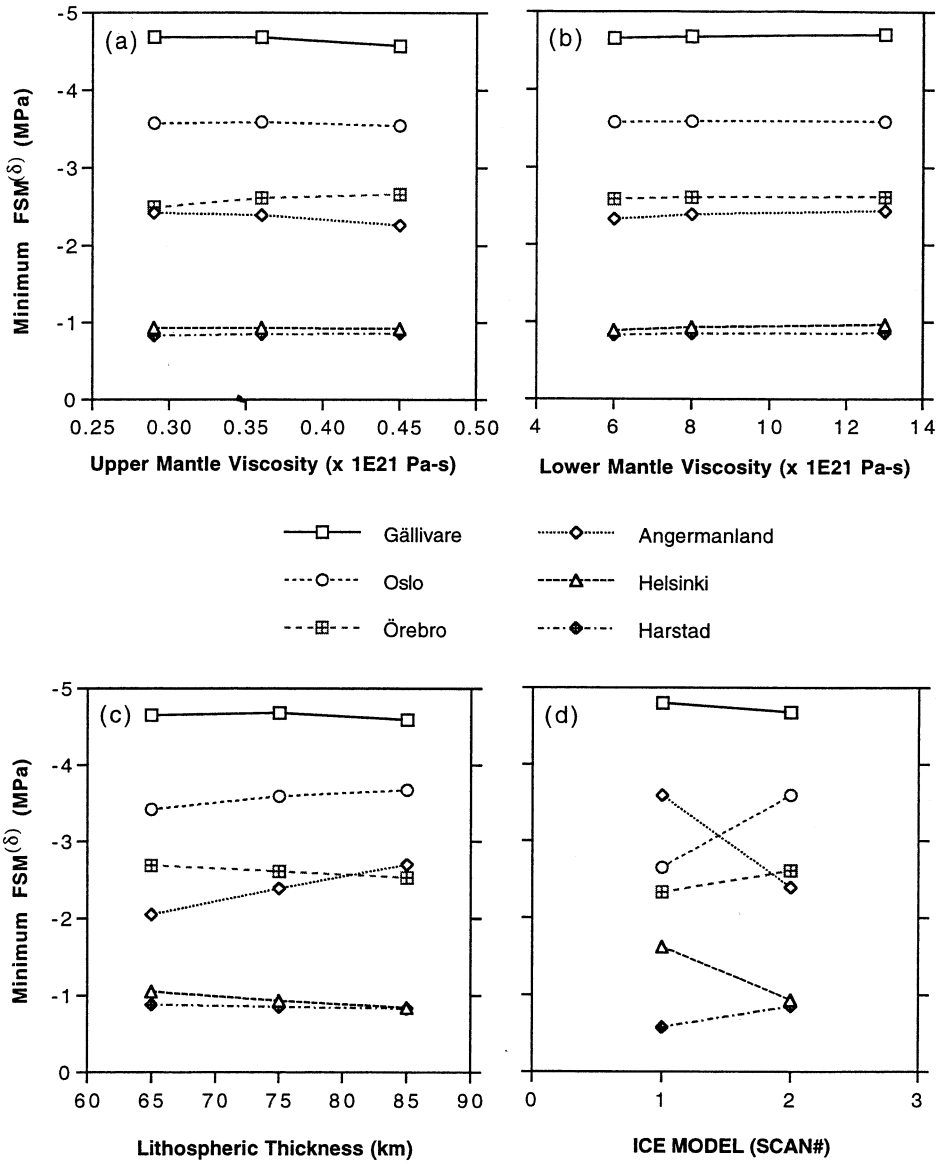

Figure 10. As Fig. 9, but for the minimum value of $FSM^{(\delta)}$.

anonymous reviewer for their useful suggestions and to the Institute of Seismology, University of Helsinki for providing the earthquake data in Fig. 1.

REFERENCES

Adams, J., 1996. Paleoseismology in Canada: a dozen years of progress, *J. geophys. Res.,* **101,** 6193–6207.

Andersen, B.G., 1981. Late Weichselian ice sheets in Eurasia and Greenland, in *The Last Great Ice Sheets,* pp. 1–65, eds Denton, G.H, & Hughes, T.J., Wiley, New York.

Arvidsson, R., 1996. Fennoscandian earthquakes: whole crust rupturing related to postglacial rebound, *Science,* **274,** 744–746.

Arvidsson, R. & Kulhanek, O., 1994. Seismodynamics of Sweden deduced from earthquake focal mechanisms, *Geophys. J. Int.,* **116,** 377–392.

Bungum, H., 1989. Earthquake occurrence and seismotectonics in Norway and surrounding areas, in *Earthquakes at North-Atlantic Passive Margins: Neotectonics and Postglacial Rebound,* pp. 501–519, eds Gregersen, S. & Basham, P.W., Kluwer, Dordrecht.

Bungum, H., Alsaker, A. & Kvamme, L.B. & Hansen, R.A., 1991. Seismicity and seismotectonics of Norway and nearby continental shelf areas, *J. geophys. Res.,* **96,** 2249–2265.

Clauss, B., Marquardt, G. & Fuchs, K., 1989. Stress orientations in the North Sea and Fennoscandia, a comparison to the central European stress field, in *Earthquakes at North-Atlantic Passive Margins: Neotectonics and Postglacial Rebound,* pp. 277–287, eds Gregersen, S. & Basham, P.W., Kluwer, Dordrecht.

Davenport, C.A., Ringrose, P.S., Becker, A., Hancock, P. & Fenton, C., 1989. Geological investigations of late and post glacial earthquake activity in Scotland, in *Earthquakes at North-Atlantic Passive Margins: Neotectonics and Postglacial Rebound,* pp. 175–194, eds Gregersen, S. & Basham, P.W., Kluwer, Dordrecht.

Denton, G.H. & Hughes, T.J., eds, 1981. *The Last Great Ice Sheets,* Wiley, New York.

Dziewonski, A.M. & Anderson, D.L., 1981. Preliminary reference Earth model, *Phys. Earth planet. Inter.,* **25,** 297–356.

Ekamn, M., 1988. Gaussian curvature of postglacial rebound and the discovery of caves created by major earthquakes in Fennoscandia, *Geophysica,* **24,** 47–56.

Ekman, M., 1985. Gaussian and mean curvatures of Earth tides and postglacial land uplift, and their effects on earthquakes, *PhD thesis,* University of Uppsala.

Gregersen, S. & Basham, P.W., 1989. Summary, Conclusions and Recommendations, in *Earthquakes at North-Atlantic Passive Margins: Neotectonics and Postglacial Rebound,* pp. 1–6, eds Gregersen, S. & Basham, P.W., Kluwer, Dordrecht.

Johnston, A.C., 1987. Suppression of earthquakes by large continental ice sheets, *Nature,* **330,** 467–469.

Johnston, A.C., 1989. The effects of large ice sheets on earthquake genesis, in *Earthquakes at North-Atlantic Passive Margins: Neotectonics and Postglacial Rebound,* pp. 581–599, eds Gregersen, S. & Basham, P.W., Kluwer, Dordrecht.

Johnston, P., Wu, P. & Lambeck, K., 1998. Dependence of horizontal stress magnitude on load dimension in glacial rebound models, *Geophys. J. Int.,* **132,** 41–60.

Johnston, P., Wu, P. & Lambeck, K., 1999. Glacial rebound and seismicity in Scotland, *Q. Sci. Rev.,* submitted.

Kleman, J., Hättestrand, C., Borgström, I. & Stroeven, A., 1997. Fennoscandian palaeoglaciology reconstructed using a glacial geological inversion model, *J. Glaciol.,* **43,** 283–299.

Kujansuu, R., 1964. Nuorista siirroksista Lapissa, *Geologi,* **16,** 30–36.

Lagerbäck, R., 1978. Neotectonic structures in northern Sweden, *Geologiska Föreningens i Stockholm Förhandlingar,* **100,** 263–269.

Lagerbäck, R. & Witschard, F., 1983. Neotectonics in northern Sweden—geological investigations, *Geol. Surv. Sweden, Techn. Rept,* 83–58, 1–58.

Lambeck, K., 1995. Late Devensian and Holocene shorelines of the British Isles and North Sea from models of glacio-hydro-isostatic rebound, *J. geol. Soc. Lond.,* **152,** 437–448.

Lambeck, K., 1999. Shoreline displacements in southern-central Sweden and the evolution of the Baltic Sea since the last maximum glaciation, *J. geol. Soc. Lond.,* **156,** 465–486.

Lambeck, K., Johnston, P. & Nakada, M., 1990. Holocene glacial rebound and sea-level change in NW Europe, *Geophys. J. Int.,* **103,** 451–468.

Lambeck, K., Smither, C. & Johnston, P., 1998a. Sea-level change, glacial rebound and mantle viscosity for northern Europe, *Geophys. J. Int.,* **134,** 102–144.

Lambeck, K.C., Smither & Ekman, M., 1998b. Tests of glacial rebound models for Fennoscandinavia based on instrumented sea- and lake-level records, *Geophys. J. Int.,* **135,** 375–387.

Lambeck, K., 1993. Glacial rebound of the British Isles—II. A high resolution, high-precision model, *Geophys. J. Int.,* **115,** 960–990.

Lundqvist, J. & Lagerbäck, R., 1976. The Pärve fault: a late-glacial fault in the Precambrian of Swedish Lapland, *Geol. Fören. Stockholm Förh.,* **98,** 45.

Mitrovica, J.X., 1996. Haskell [1935] revisited, *J. geophys. Res.,* **101,** 555–569.

Mitrovica, J.X. & Peltier, W.R., 1991. On postglacial geoid subsidence over the equatorial oceans, *J. geophys. Res.,* **96,** 20 053–20 071.

Muir Wood, R., 1989. Extraordinary deglaciation reverse faulting in northern FennoScandia. in *Earthquakes at North-Atlantic Passive Margins: Neotectonics and Postglacial Rebound,* pp. 141–173, eds Gregersen, S. & Basham, P.W., Kluwer, Dordrecht.

Paterson, W.S.B., 1981. *The Physics of Glaciers,* Pergamon Press, Toronto.

Pedersen, S.S., 1995. *Israndslinier i Norden,* Danm. Geol. Unders., Copenhagen.

Rohrman, M., Van der Beek, P., Andriessen, P. & Cloetingh, S., 1995. Meso-Cenozoic morphotectonic evolution of Southern Norway—Neogene domal uplift inferred from apatite fission track thermochronology, *Tectonics,* **14,** 703–718.

Shilts, W.W., Rappol, M. & Blais, A., 1992. Evidence of late and postglacial seismic activity in the Temiscouata-Madawaska Valley, Quebec—New Brunswick, Canada, *Can. J. Earth Sci.,* **29,** 1043–1059.

Skordas, E. & Kulhanek, O., 1992. Spatial and temporal variations of Fennoscandian seismicity, *Geophys. J. Int.,* **111,** 577–588.

Slunga, R.S., 1989. Focal mechanisms and crustal stresses in the Baltic Shield, in *Earthquakes at North-Atlantic Passive Margins: Neotectonics and Postglacial Rebound,* pp. 261–276, eds Gregersen, S. & Basham, P.W., Kluwer, Dordrecht.

Spada, G., Yuen, D.A., Sabadini, R. & Boschi, E., 1991. Lower-mantle viscosity constrained by seismicity around deglaciated regions, *Nature,* **351,** 53–55.

Stephansson, O., 1989. Stress Measurements and modeling of crustal rock mechanics in Fennoscandia, in *Earthquakes at North-Atlantic Passive Margins: Neotectonics and Postglacial Rebound,* pp. 213–229, eds Gregersen, S. & Basham, P.W., Kluwer, Dordrecht.

Stephansson, O., 1993. Rock stress in the Fennoscandian Shield, in *Comprehensive Rock Engineering, Principles, Practice and Projects,* pp. 445–459, ed. Hudson, J.A., Pergamon Press, Oxford.

Wahlstrom, R., 1989. Seismodynamics and postglacial faulting in the Baltic Shield, in *Earthquakes at North-Atlantic Passive Margins: Neotectonics and Postglacial Rebound,* pp. 467–482, eds Gregersen, S. & Basham, P.W., Kluwer, Dordrecht.

Wu, P., 1996. Changes in orientation of near-surface stress field as constraints to lower-mantle viscosity and horizontal principal tectonic stress difference in Eastern Canada, *Geophys. Res. Lett.,* **23,** 2263–2266.

Wu, P., 1997. Effect of viscosity structure on fault potential and stress orientations in Eastern Canada, *Geophys. J. Int.,* **130,** 365–382.

Wu, P., 1998a. Will earthquake activity in eastern Canada increase in the next few thousand years? *Can. J. Earth Sci.,* **35,** 562–568.

Wu, P., 1998b. Intraplate earthquakes and postglacial rebound in Eastern Canada and Northern Europe, in *Dynamics of the Ice Age Earth: a Modern Perspective,* pp. 603–628, ed Wu, P., Trans Tech Publications, Uetikon-Zürich, Switzerland.

Wu, P. & Hasegawa, H., 1996a. Induced stresses and fault potential in Eastern Canada due to a disc load: a preliminary analysis, *Geophys. J. Int.,* **125,** 415–430.

Wu, P. & Hasegawa, H., 1996b. Induced stresses and fault potential in Eastern Canada due to a realistic load: a preliminary analysis, *Geophys. J. Int.,* **127,** 215–229.

Zoback, M.D. *et al.,* 1994. Upper crustal strength inferred from stress measurements to 6 km depth in the KTB borehole, *Nature,* **365,** 633–635.